Acta Astronautica 240 (2026) 522–529

Contents lists available at ScienceDirect

Acta Astronautica

journal homepage: www.elsevier.com/locate/actaastro

Research paper

Control allocation for over-actuated satellite laser communication systems

René Rüeddenklau [a,b,*], Georg Schitter [b]

[a] German Aerospace Center (DLR), Institute of Communications and Navigation, Münchenerstr. 20, 82234 Wessling, Germany
[b] Technische Universität Wien, Mechatronics and Power Electronics Institute (MPEI), Gusshausstr. 27-29, 1040 Vienna, Austria

ARTICLE INFO

Keywords:
Control allocation
Free-space optical communication
Multi-objective optimization
Acquisition and tracking
Beam steering
Satellite

ABSTRACT

This work proposes a methodology to optimize actuator contribution to the overall system for constellations with optical links between satellites and Earth, where multiple laser communication terminals are deployed on a common host platform to maximize link duration and enable data exchange between multiple communication nodes. To satisfy specifications regarding field of regard, bandwidth, and accuracy, a combination of dedicated actuators is employed. The strategy, known as control allocation, is tailored to meet the requirements of optical communication. The procedure considers the dynamics and constraints of each actuator, providing a comprehensive approach. It enables a modular design, including the host satellite platform itself. As a result, the allocation algorithm enables optimizations concerning power consumption, adaptation to dynamic link switching conditions, and tracking robustness compared to a decentralized approach. This is achieved by assigning disturbances to the most suitable actuator while meeting secondary objectives. Bounded non-linear weighted least squares optimization is used to account for coordinate system transformation, and a graphical tool is demonstrated to tune the involved weighting matrices in the developed multi-link scenario.

1. Introduction

Control allocation is a critical component in modern control systems, particularly when managing multiple actuators to achieve precise distribution of control. In satellite based FSOC systems with redundant or multiple actuators, such as a reaction wheel, magnetorquer, FPA and CPA, the challenge lies in efficiently distributing control efforts among the actuators to meet performance objectives while avoiding actuator saturation and ensuring system availability. These systems are called over-actuated since they provide more control effectors than control objectives. However, this enables the introduction of secondary objectives such as power consumption minimization and optimization for operating points of individual actuators.

In recent years, there has been growing interest in applying advanced control allocation techniques to improve the performance of control systems in various engineering disciplines [1]. One prominent field for applied control allocation is avionics, where it is used to control the redundant actuators of airplanes to achieve the desired attitude [2,3]. Further common disciplines include robotics to achieve multiobjective targets [4], as well as spacecraft attitude [5,6] and thrust control [7–9]. A more recent work analyzes the use case of FSOC with emphasis on adaptive optics control [10], where unmeasured outputs of an over-actuated deformable mirror are estimated using a frequency-domain-based approach. Another aspect of control allocation targets cellularized systems, that shall replace monolithic structures, for which distributed control algorithms are proposed [11–13]. This can be an extension also for optical communications system constellation. However, before dealing with multi-link, multi-system challenges, a tailored approach for current over-actuated optical communications systems has to be found.

The aforementioned engineering domains show that control allocation can be used as an inter-disciplinary tool to resolve non-unique solutions. Future FSOC systems for space applications will be used to relay large amounts of data in classical communication, but also enable coherent time transfer and ranging applications, as well as quantum key distribution [14]. A major challenge in all optical communication scenarios is ensuring precise and efficient pointing, acquisition and tracking (PAT) capabilities. The host satellite platform's body pointing provides fundamental accuracy for attitude knowledge and control. This accuracy is enhanced by using dedicated actuators in the optical communication system. An FPA is used to steer the laser beam precisely using optical feedback from a dedicated tracking sensor. The FPA also provides a higher control bandwidth, up to the kilohertz regime. Additionally, a CPA can be used to extend the field of regard (FOR) to point with fewer constraints on the satellite orientation. The number of actuators demand a control strategy that considers their respective dynamic performance characteristics and limitations to make optimal use

* Corresponding author at: German Aerospace Center (DLR), Institute of Communications and Navigation, Münchenerstr. 20, 82234 Wessling, Germany.
E-mail addresses: rene.rueddenklau@dlr.de (R. Rüeddenklau), schitter@acin.tuwien.ac.at (G. Schitter).

https://doi.org/10.1016/j.actaastro.2025.12.026
Received 26 September 2025; Received in revised form 12 November 2025; Accepted 11 December 2025
Available online 15 December 2025

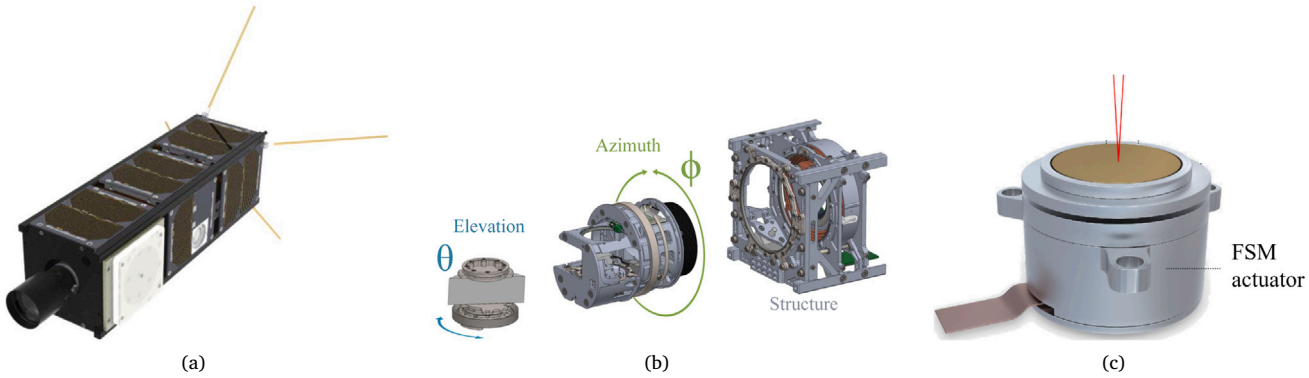

Fig. 1. Representative illustrations of FSOC subsystems with (a) an integrated 3U CubeSat, (b) an exploded view of a CPA, built in a gimbaled prism configuration, and (c) a HRA type of FSM [16].

of them. The process of control allocation becomes even more relevant when considering multi-link scenarios for satellite constellations where separate pointing objectives have to be met. Particularly the principle of dynamic control allocation [15] implies advantages for the envisaged use case of FSOC in a satellite constellation, specifically for CubeSats which allow lower cost missions but also suffer from reduced attitude control performance compared to larger satellites.

This paper focuses on the development and evaluation of control allocation strategies tailored to the unique requirements for an over-actuated, satellite-based laser communication terminal (LCT). The main contributions are the introduction of new optimization objectives relevant to the application and a non-linear weighted least squares algorithm that accounts for coordinate transformations. A graphical approach is proposed, that tunes the weighting parameters between the objectives based on the characteristics of the actuator employed. Further, currently available beam steering subsystems are used to explore the range, bandwidth and accuracy Pareto front of over-actuated laser communication systems. Through a simulated multi-link scenario performance analysis, it is demonstrated how these advanced control allocation techniques can maintain pointing accuracy, while significantly reducing energy consumption, and simplify the tuning of interdependent subsystems, contributing to the reliability and adaptability of next-generation satellite communication systems.

Section 2 explores the requirements for free-space optical communications systems and estimates limitations of state-of-the-art beam steering actuators. Further, new secondary objectives are formulated and integrated within the dynamic control allocation which is extended to non-linear use cases. In Section 3, the effectiveness of the identified weighting combination is analyzed when using a sample secondary objective compared to an equally weighted multi-link scenario.

2. Control allocation extension for free-space optical communications

To understand the need to adapt general control allocation approaches to FSOC, the following section first introduces the subsystems that are commonly employed for establishing space-based optical links. Then, considerations for an optical link are analyzed with respect to how they can be addressed by control allocation. Then, control laws are formulated, and the non-linear treatment of the least-squares optimization is introduced to account for coordinate system rotations and transformations.

2.1. Laser communication systems

The number of optical communication terminals in space increases continuously [17]. This is also due to the number of planned and active constellations [18,19]. Especially this type of application demands for multiple communication terminals, hosted on a common satellite platform. Although all optical terminals are subject to design changes involving the actuators used, three common types are used throughout the systems and are described in the following section.

2.1.1. Typical subsystems for space-based free-space optical communications

The use of FSOC systems on flying objects such as zeppelins, high altitude platforms, airplanes or satellites is advantageous because large distances can be covered without obstacles and thus contribute to a more effectively usable range. Therefore, LCTs are often located on a host platform, which in turn can be used for body pointing to align the beam. This work will focus on satellite based scenarios. However, the developed method can be applied to all other mentioned areas of application. Therefore, a satellite is included as a representative effector in this scenario as seen in Fig. 1. In addition, the conventional subsystems a CPA and a FPA are depicted.

Including the satellite and its ADCS in this consideration makes particular sense since the spacecraft can adjust its attitude independently of its orbital movement. A satellite also offers the possibility of accommodating several LCTs in order to be used to establish inter-satellite links and similarly make contact with an optical ground station (see Fig. 2). In common designs, an LCT consists of an FPA and a CPA, whereby the CPA extends the effective pointing range and the FPA is used to enable precise alignment and to compensate for high-frequency disturbance due to its low inertia [20]. However, these systems can be supplemented by other actuators wherever dedicated systems are necessary, for example coupling into a fiber or adjusting the point ahead angle for signal runtime compensation. It is also common to use multiple sources of reference to determine and align the pointing attitude. Thus, inertial measuring units, horizon and sun sensors and magnetometers are available on a satellite. Furthermore, an LCT usually relies on a dedicated tracking sensor such as a quadrant-photodiode [21], a position sensitive device [22] or a focal plane array [23] to identify the incoming beacon or data signal. This tracking sensor can also consist of two sensors with differing field of view (FOV) and, hence, achievable angular resolution in order to first acquire the signal faster and then switch to track it precisely [24]. Control allocation can account for multiple sensors by weighting the relevance of each input according to the pointing phase and the most trustworthy information at the time. In summary, in a system with over-actuation, achieving multiple pointing targets is essential given the availability of actuators with different dynamics and alignment sources with varying degrees of accuracy.

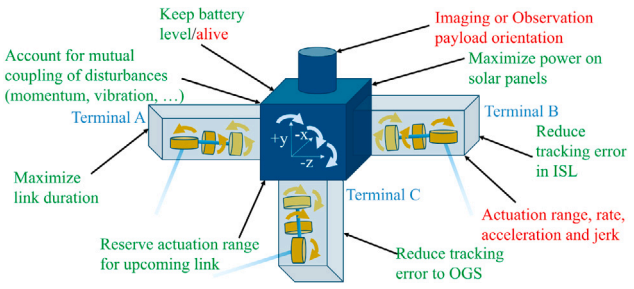

Fig. 2. Considerations for optimizing (green) the control allocation of a typical space laser communication system while accounting for the constraints (red). (For interpretation of the references to color in this figure legend, the reader is referred to the web version of this article.)

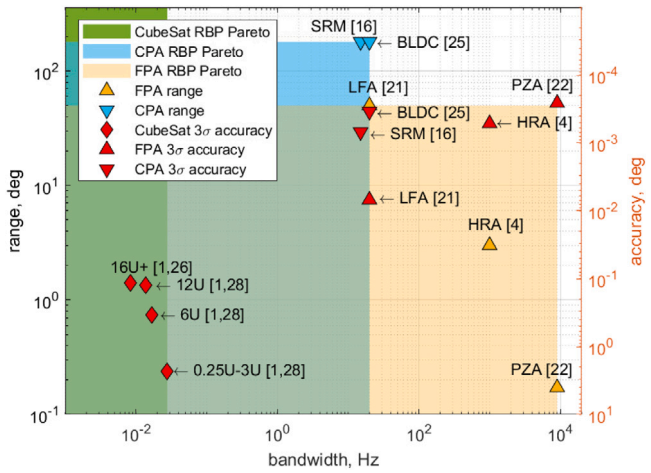

Fig. 3. The actuator Pareto front displaying the range-bandwidth space that can be covered by state-of-the-art technologies. It includes the achievable accuracy of these technologies according to literature, and each technology is separated in the dedicated FPA, CPA, and CubeSat ADCS subsystems. (For interpretation of the references to color in this figure legend, the reader is referred to the web version of this article.)

2.1.2. Considerations for adaptation to laser communication terminals

The advantage of an over-actuated system is, that it can be utilized to achieve secondary objectives. Requirements can therefore be divided into constraints and optimizations. Constraints must always be adhered to, as they are caused by the needs of the systems used, or are essential for achieving the primary objective. Fig. 2 shows examples of such constraints and optimizations for the defined scenario. For example, it is important to adhere to the effective range of the actuators, which can be design or environmentally driven. Furthermore, the top priority must be to keep the optical link stable. However, it may be that other payloads have to be taken into account and have priority, for instance because an image has to be captured by a camera at a certain point in time.

Optimizations may involve power consumption optimization, operating point optimization for an actuator, or avoiding commands that would lead to increased wear. Additionally, if a critical battery limit is reached, this optimization parameter may become a constraint, prioritizing the alignment of the solar panels and avoidance of high power consumption levels. It may be required to use optimization to reserve an actuation range for a future planned link whose calculated range requirements in combination with the dynamics would otherwise lie outside the capabilities of the actuator set.

In the following, capabilities of state-of-the art actuators are used to define the currently, technically achievable range-bandwidth product (RBP) Pareto front [25] for the three envisaged subsystems (see Fig. 3). The results are plotted to mark an area of the range-bandwidth design space (blue and orange triangles) as well as the achievable accuracy (red triangles) linked to the same actuator reference. Note that CubeSat range data points are not shown since they can rotate freely. It is well visible that all three types of actuators do share bandwidth and range areas. However, actuators with broad range capabilities tend to have reduced accuracy and bandwidth, and vice versa. This illustrates why combining dedicated actuators with an over-actuated system may be required. Another aspect to consider is the previously mentioned secondary objectives. The influence of the newly introduced optimization parameters depends on the dynamics and limitations of each actuator. A combination of these would benefit from an FPA with a higher range while maintaining high bandwidth and, therefore, an increased RBP. Conversely, a CPA can support scenarios where the resulting tracking accuracy is sufficient for mission goals and less bandwidth is needed. However, aspects such as the cost and size of the system must also be considered in real-world applications.

Constraints and performance based on the identified Pareto front are used for later analysis in Section 3. Note that the following analysis assumes working low-level controller implementations. Therefore, the following selection was made. First of all the satellite and its ADCS [17]. It is the one system with, theoretically, unlimited range, since only sun avoidance angle and power budget constraints hinder it from pointing into arbitrary directions. Its low-level controller is considered a given third-party, black-box implementation where only the dynamics and limitations are known. Bandwidths are derived from Blue Canyon Technologies [26], since they provide satellite buses in all categories from 3 $\mathrm{deg\,s^{-1}}$ to 10 $\mathrm{deg\,s^{-1}}$. The accuracy of the three categories was derived by the mean 3σ result of all current platforms listed in NASA's state-of-the-art small spacecraft technology report [17], which results in 2.296 deg, 0.340 deg, 0.124 deg and 0.117 deg from the smallest to the largest category. The CPA is considered to be a hemispherical, gimbal implementation in this scenario, since it offers the most flexibility for pointing and allows compact integration. Brushless-DC motors [20] or switched reluctance motors [27] are employed to drive the mechanism, reaching tracking bandwidths of about 20 Hz while providing a large pointing range. A standard servo-controller [20] is assumed as low-level implementation using encoders for position and velocity control, whose accuracy depends on the demanded tracking dynamics and can reach $3.4 \cdot 10^{-4}$ deg (3σ). Lastly, the FSM which is assumed to feature closed-loop capabilities by angular sensors. The HRA technology reaches the highest RBP [25] allowing 3 deg mechanical range while maintaining precise pointing control [28] with a tracking bandwidth of 1 kHz and an accuracy of $5.16 \cdot 10^{-4}$ deg (3σ). The piezo electric actuator (PZA) [29] and the lorentz force actuator (LFA) [30] are alternatives that have distinct advantages depending on the use case. They achieve higher bandwidths up to 10 kHz at the cost of lower ranges, and vice versa with ranges up to 50 deg. The low-level control architecture is usually a classical proportional–integral–derivative (PID) implementation [31].

The primary objective of the allocation controller is to minimize tracking error. This means that it should not contribute to the overall error budget due to computational inaccuracies or delays. During different phases like acquisition or tracking, sources might switch depending on their availability and quality of data. Ephemeris data, which is gathered by the ADCS, is most certainly available but suffers from limited accuracy and is often sampled at a low rate. Wide-field of view (WFOV) sensors are sometimes used, when the FOV needs to be increased during the acquisition process and can therefore be used to transition from ephemeris based pointing to coarse pointing [24]. The narrow-field of view (NFOV) sensor yields the most accurate measurements and can typically be sampled at a high rate, often up to the kilohertz regime. The minimum feasible tracking error mostly depends on this device.

Although the specific capabilities of the different subsystems can vary between missions, general measures of performance can be derived:

- tracking error (Mean, STD, RMS),
- duration of tracking within links,
- quality of achieved secondary optimization objectives.

Due to the over-actuated scenario, additional secondary objectives specific to FSOC applications can be introduced:

- power consumption,
- wear and tear,
- reserved angular range,
- self emitted disturbance.

Their feasibility is influenced by three main factors:

- optimization solver used,
- tuning of weighting matrices,
- used actuators.

2.2. Adapting control allocation

As previously mentioned, control allocation methods are well-known and proven implementations in other engineering disciplines [1]. However, some adaptations are necessary to make them better suited for FSOC applications. First of all, new objectives are introduced, then a representative over-actuated scenario is defined. It is used to improve the choice of the solver, since it has to work with non-linear effectiveness matrices due to inherent rotations inside the system and specifically for the CPA which uses spherical coordinates in the chosen configuration [20].

2.2.1. Control laws

In general, the allocation tries to optimize the control effort based on the control input u and its derivatives. Each term can be scaled by a constant or function and all dimensions can be weighted by dedicated matrices W_i

$$u(t) = \arg\min \left\{ \|W_1[u(t) - u_s(t)]\|^2 + \|W_2[u(t) - u(t-T)]\|^2 \right\}. \tag{1}$$

Further, it tries to follow the commanded input with the distributed virtual control v taking the effectiveness of each and every actuator into account. The problem can be described by a bounded least-squares formulation that considers actuator constraints as well

$$\Omega = \arg\min \|W_v[Bu(t) - v]\|, \quad \text{subject to } u_{\min} \le u \le u_{\max}. \tag{2}$$

Since optimization goals do not only depend on the commanded position and velocity, but also on the acceleration and jerk, the formulation of additional cost functions is performed in the following. Another term that is relevant to this discussion is the time aspect, given that links—particularly those between different planes—can exhibit significant dynamics due to the presence of high relative velocities. Therefore, actuator range can be reserved by considering time to the next planned link event and the remaining distance of the actuator to the new start orientation.

Eq. (4a) involves R, which is in general a resistance leading to a current which will be withdrawn from the battery. For a brushless-DC motor the resulting current draw can be estimated as

$$M = K_t \cdot i, \tag{3a}$$

$$M = J \cdot \dot{\omega}, \tag{3b}$$

$$R = \frac{J}{K_t}, \tag{3c}$$

with $\dot{\omega} = \ddot{u}$, K_t motor constant and J inertia. In Eq. (4b) the wear and tear caused by jerk is a relevant factor when operating direct drive gimbals. However, a general dependency between wear and jerk is not trivial to derive. As a general optimization goal, a minimization of the jerk is preferable [32]. Eq. (4c) is used to reserve range for an upcoming link, where u_n is the next target pointing needed for establishing the upcoming link, compared to the actual pointing command u. The term becomes more important the closer the starting time of the link window t_0 is to the actual time t. It becomes irrelevant as soon as the link has started. In Eq. (4d) the factor g_k is a measured function or lookup table that accounts for introduced disturbance of a system depending on the velocity. An example can be the velocity dependent harmonic resonance of a reaction wheel rotation [33].

$$u_{\text{pow}}(t) = \arg\min \|W_3[R\ddot{u}(t)]\|^2, \quad \text{subject to } E_{\min} \le E_{\text{bat}} - \Sigma(R\ddot{u}) \le E_{\max}, \tag{4a}$$

$$u_{\text{taw}}(t) = \arg\min \|W_4[f_F \ddot{u}(t)]\|^2, \tag{4b}$$

$$u_{\text{ran}}(t) = \arg\min \left\| W_5 \left[\underbrace{\frac{1}{t - t_0 + 1}}_{T} (u - u_n) \right] \right\|^2, \tag{4c}$$

$$u_{\text{dis}}(t) = \arg\min \|W_6[g_k \dot{u}(t)]\|^2. \tag{4d}$$

2.2.2. Scenario model formulation

For a more practical investigation of the control allocation algorithm, a constraint scenario of a constellation of three satellites and one ground station is modeled. The selected constellation results in possibilities for an ISL regarding terminals A and B and a simultaneous DTE link for terminal C (see Fig. 2).

Having described the influence of configuration parameters such as the weighting matrices in Section 2.1.2, the composition of the effectiveness matrix B can be derived. The matrix includes the influence of each manipulated variable u_i on the corresponding control variable v_j and is described by the respective partial derivatives

$$B_{ij} = \frac{\partial v_j}{\partial u_i}. \tag{5}$$

The matrix B needs to be recalculated for each iteration which includes the partial derivative of the function for the vector components with respect to the current system orientation. Both, the satellite rotation and the tip and tilt angles of the terminals are taken into account. The current orientation of a terminal results from rotation of the unit vector normal to the surface of the satellite. The following example applies to terminal A

$$\partial v_{\text{A,IRF}} = R_{\text{S}}(\phi_x, \phi_y, \phi_z) \cdot R_{\text{A}}(\phi_{x,\text{A}}, \phi_{y,\text{A}}) \cdot (0\ 0\ 1)^{\text{T}}_{\text{BRF}}. \tag{6}$$

R_{sat} and R_{A} are made up of the product of the rotation matrices for the respective rotation axes. To calculate the partial derivative, the rotation matrix of the corresponding actuator is differentiated. Taking into account the chain rule, the partial derivative of the control command v_{A} after the rotation of the satellite around the y-axis results in

$$\frac{\partial v_{\text{A}}}{\partial \phi_y} = \frac{\partial R_{\text{S}}}{\partial \phi_y} \cdot R_{\text{A}} \cdot (0\ 0\ 1)^{\text{T}}_{\text{BRF}} = R_z(\phi_z) \cdot \frac{\partial R_y(\phi_y)}{\partial \phi_y} \cdot R_x(\phi_x) \cdot R_{\text{A}} \cdot (0\ 0\ 1)^{\text{T}}_{\text{BRF}}. \tag{7}$$

Similarly, all other entries of the effectiveness matrix are formed by partial derivatives of the respective control variables according to the associated manipulated variables. As the actuators of a terminal have no direct influence on external control variables, a zero effectiveness can be assigned to the corresponding entries of the matrix. The complete matrix B thus results in

$$B = \begin{bmatrix} \frac{\partial v_{\text{A}}}{\partial \phi_{x,\text{S}}} & \frac{\partial v_{\text{A}}}{\partial \phi_{y,\text{S}}} & \frac{\partial v_{\text{A}}}{\partial \phi_{z,\text{S}}} \\ \frac{\partial v_{\text{B}}}{\partial \phi_{x,\text{S}}} & \frac{\partial v_{\text{B}}}{\partial \phi_{y,\text{S}}} & \frac{\partial v_{\text{B}}}{\partial \phi_{z,\text{S}}} \\ \frac{\partial v_{\text{C}}}{\partial \phi_{x,\text{S}}} & \frac{\partial v_{\text{C}}}{\partial \phi_{y,\text{S}}} & \frac{\partial v_{\text{C}}}{\partial \phi_{z,\text{S}}} \end{bmatrix}$$

$$\begin{bmatrix} \frac{\partial v_A}{\partial \phi_{x,A}} & \frac{\partial v_A}{\partial \phi_{y,A}} & 0 & 0 & 0 & 0 \\ 0 & 0 & \frac{\partial v_B}{\partial \phi_{x,B}} & \frac{\partial v_B}{\partial \phi_{y,B}} & 0 & 0 \\ 0 & 0 & 0 & 0 & \frac{\partial v_C}{\partial \phi_{x,C}} & \frac{\partial v_C}{\partial \phi_{z,C}} \end{bmatrix}. \tag{8}$$

2.2.3. Non-linear control effectiveness

The baseline work [15] uses a bounded linear weighted least squares (WLS) approach to solve the optimization problem. However, due to the coordinate system transformations, non-linear behavior of the effectiveness matrix B is inherent. An additional non-linearity originates from the CPA which is assumed to be arranged in an azimuth and an elevation axis configuration. This introduces the need to command pointing angles in a spherical coordinate system. Transformations between cartesian and spherical coordinates in turn necessitate trigonometric functions for transformation as described in Algorithm 1. Please note that W_2 has been replaced by the newly introduced W_6, which incorporates the angular rate already. This means that the virtual control command v has a dependency of time t and input u, which influence the effectiveness value in B

$$v = h(u, x, t) = B(x, t) \cdot u. \tag{9}$$

When linearizing this effectiveness around the current operating point, as done by the WLS method, errors do occur, reducing the accuracy of the control command. To mitigate the remaining errors, a non-linear optimization approach based on the Levenberg–Marquardt algorithm is considered below [34,35]. The problem formulation

$$\min_x \|f(x)\|_2^2 = \min_x \left(f_1(x)^2 + \cdots + f_n(x)^2\right), \tag{10}$$

allows problems to be solved according to the least-squares method subject to defined constraints. The non-linear weighted least squares (NLWLS) formulation is computed on an error function (see Alg. 1) that calculates the error based on the actual alignment.

Algorithm 1 Calculate non-linear relationship and errors with applied weighting.

Require: $v, u, u_s, W_i, \alpha, \phi, \theta$
Ensure: error e
  Calculate derivatives of u:
    $u^{(1)} \leftarrow \frac{d}{dt}u$
    $u^{(2)} \leftarrow \frac{d^2}{dt^2}u$
    $u^{(3)} \leftarrow \frac{d^3}{dt^3}u$
  Calculate rotation matrices $T(\alpha)$ **for each unit and spherical to cartesian transform** $S(\phi, \theta)$
  $u_{A,B} \leftarrow T_{A,B}(\alpha) \cdot u_{A,B}$
  $u_C \leftarrow T_C(\alpha) \cdot S(\phi, \theta) \cdot u_C$
  Calculate error e:
  $e_1 \leftarrow W_v \cdot (u - v)$
  $e_2 \leftarrow W_1 \cdot (u - u_s)$
  $e_3 \leftarrow W_3 \cdot u_{\text{pow}}(u^{(2)}, u)$
  $e_4 \leftarrow W_4 \cdot u_{\text{taw}}(u^{(3)})$
  $e_5 \leftarrow W_5 \cdot u_{\text{ran}}(t)$
  $e_6 \leftarrow W_6 \cdot u_{\text{dis}}(u^{(1)})$
  return $e = [e_1, e_2, e_3, e_4, e_5, e_6]$

The algorithm defines the non-linear residual error function used in the allocation problem. The convergence properties therefore follow from the Levenberg–Marquardt algorithm, which under the usual smoothness and full-rank Jacobian assumptions ensures local convergence to a stationary point of the non-linear least-squares cost. As the underlying second-order actuator dynamics are smooth, these assumptions are satisfied in the considered setting. The current manipulated variables—satellite rotations and deflection angles of the LCT—are converted into rotation matrices, from which the effective current pointing direction of the terminals is determined. The error is combined of all defined cost functions described in Section 2.2.1.

Table 1
Scenario parameters and boundaries.

Parameter	FPA	CPA	SAT
Range u_{lim}, deg	±4	±90	±180
Rate $\dot{u}_{\text{lim}}$, deg s^{-1}	100	36	10
Power R, a.u.	0.5	0.0267	0.1716
Δu_{target}, deg	$\begin{pmatrix}0.30\\0.01\\0\end{pmatrix}$	$\begin{pmatrix}-0.25\\-0.01\\0\end{pmatrix}$	$\begin{pmatrix}0.05\\0\\0.30\end{pmatrix}$

3. Performance simulation and analysis

In order to demonstrate the working principle of the proposed changes to adapt to an FSOC scenario, the selected configuration of actuators (see Table 1) is used to determine the normalized cost functions in order to pre-select an initial weighting. It is important to bear in mind that R is based on the deflection u for the FPA and on the acceleration ü for the CPA and the spacecraft. Note that the attitude determination is assumed to be free of additional disturbances in order to extract the errors introduced by the control allocation computations. This weighting set is then used to calculate the control allocation distribution for a simple step input. Finally, the influence of the power cost function is evaluated and how this influences peak-to-peak as well as mean power draw while maintaining pointing performance.

3.1. Applied graphical weight tuning by cost function normalization

The weighting matrices W_i yield a parameter set for tuning the behavior of the NLWLS control allocation algorithm in the application. Due to the multiple degrees of freedom of an over-actuated system and the introduction of new optimization objectives, it is important to derive a starting point for the weighting matrices. The graphical approach shown below illustrates how to find an initial starting point for fine tuning. All cost functions are calculated for three arbitrary sample periods ranging from a phase of constant acceleration, to constant velocity, to constant attitude in the final sample period. Thus, all dynamic stages during a link are covered, and the influence on the cost function can be evaluated.

To compare the influence of the actuators, they are normalized to the maximum value. A starting point is established by incorporating scalars, functions, or look-up tables into the parameters presented in Eqs. (4a) to (4d). According to the resulting graphs, the weighting can be chosen so that the cost function behaves as desired for the dedicated mission in all three phases. Fig. 4 plots a scenario of different phases.

Most influence on the FPA is imposed by the limitation of its range. Therefore, a steady-state position close to the center deflection is desirable at all times. Depending on the actuator technology, this orientation may be additionally preferable due to higher power consumption at larger deflection angles. In contrast, it is important for the CPA that sudden changes in acceleration, and therefore high jerks, are minimized to reduce wear and tear on the gimbal's bearings, as well as peak power consumption, as seen in the spikes between sudden changes in the sample dynamic period. Additionally, range shall be reserved for an upcoming link, which becomes more important the closer it gets to the target time point t_0, which is indicated by the end of phase three. The same is true for the satellite ADCS. However, due to a lower bandwidth, sudden accelerations are not possible, resulting in smoother gradients in the cost function. Due to its higher mass, vibration is considered a major factor, which originates from the rotation speed dependent harmonics of the reaction wheels in this scenario. Table 2 contains the resulting weighting factors, whose influence is displayed in Fig. 4. Afterward, they are used as the optimized configuration (opt) for the corresponding simulation which delivered the result for Table 3.

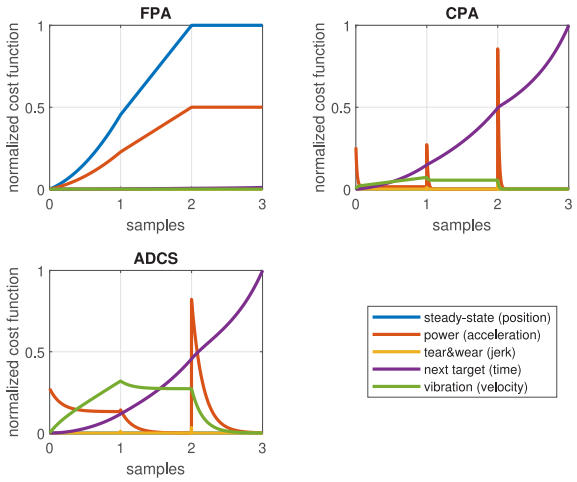

Fig. 4. Secondary objectives according to normalized weighting. The defined phases are (0–1) constant acceleration, (1–2) constant velocity and (2–3) constant position.

Table 2
Optimized weighting factors according to the graphical evaluation of the secondary objectives.

Weighting	FPA	CPA	SAT
W_u	0	0	0
W_v	1	10^{-3}	10^{-4}
$W_3 R$	0.5	$2.655 \cdot 10^9$	$1.207 \cdot 10^9$
$W_4 f_F$	0	10^3	10^4
$W_5 T(t)$	$\frac{1}{(100 \cdot (t-4))}$	$\frac{1}{4-t}$	$\frac{1}{4-t}$
$W_6 g_K$	0	10^2	$5 \cdot 10^2$

3.2. Multi-terminal non-linear constrained control allocation

In the following, the scenario is simulated using the identified weighting factors. Fig. 5 shows the simulation results for the case of equal weighting of all three terminals and alternatively for the newly introduced cost functions, where the power consumption influence is used for this demonstration. The limited FOR of terminals A and B is a constraint, as excessive rotation of the satellite would interrupt the ISL. Therefore, large rotations of satellite and CPA are needed. However, when power consumption is introduced as an additional objective, it can be shown that the target can be reached with reduced consumption while keeping the primary objectives largely unchanged. Resulting errors from numerical inaccuracies will be mitigated by the feedback loop of the built-in optical sensor—like a quadrant-photo-diode—to the microradian level. Note that the mentioned mean error e includes the period until the tracking error has settled.

In practice, it is often desirable to minimize power draw on a small CubeSat platform, since they can accommodate only a limited amount of battery capacity. However, it should be noted that other effects need to be considered as well for an entire mission duration. For example, continuously offloading the FPA will affect the CPA's lifespan due to increased wear and tear. This will have less of an effect on a CubeSat mission in low Earth orbit (LEO) since they typically last a maximum of five years. For longer missions, it is desirable to give more weight to the $W_4 f_F$ factor to counteract the expected degradation of the CPA's performance. Another aspect comes into play when scheduling a dynamic inter-plane link. If the goal is to maximize the duration of the planned link, it is desirable to give more weight to W_5. To keep the scenario comprehensible, only the influence of the u_{pow} component is analyzed in more detail in Fig. 6.

To quantitatively evaluate the changes in the acquisition and tracking process, the mean and peak-to-peak power consumption of terminal

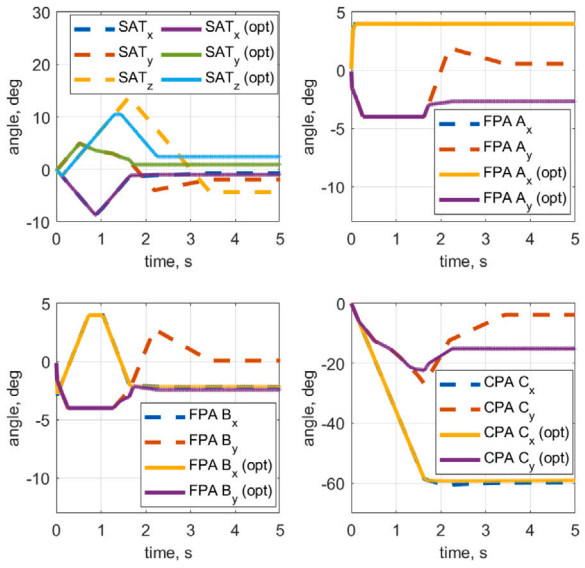

Fig. 5. Allocated control commands with (power) and without (equal) optimization for power consumption according to configuration in Table 2.

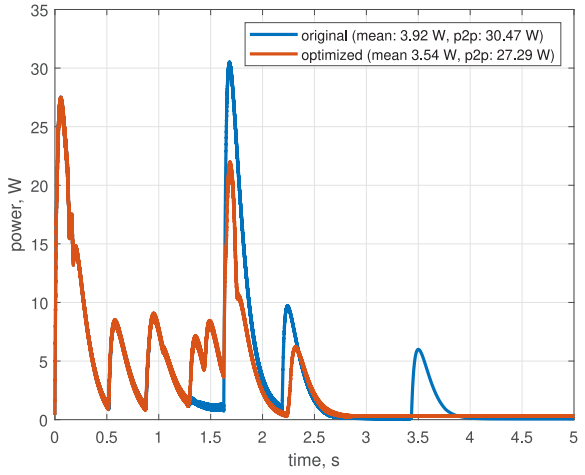

Fig. 6. Cumulative power consumption with mean and peak-to-peak (p2p) values of the considered ADCS, CPA and two FPAs configuration performing a simultaneous DTE and two intra-plane ISLs.

C are analyzed next to the overall mean pointing error, the time to acquisition of signal (AOS) and the mean offset deflection of the range limited FPA (see Table 3). The mean pointing error is calculated over the entire five seconds of the simulation, not just during the tracking phase, to account for the time it takes to settle from the initial pointing error to the delta target position within this metric. It should be noted that the linear WLS was also computed, but lead to errors beyond the FOV of the terminals and was therefore not considered further. When emphasizing only power consumption the peak-to-peak consumption can be reduced from 30.5 A to 26.9 A and mean from 3.9 A to 3.5 A over the simulated 5 s period. On the other side this led to a worse acquisition and tracking performance. Therefore, a more balanced set of weighting factors according to Table 2 is applied. Which still leads to a reduction in power consumption of 27.3 A peak-to-peak and a mean of 3.5 A while maintaining the reference pointing performance. Additionally, the settled tracking error stays within the microradian level. Another aspect to consider is the mean deflection angle of the FPA. The magnitude slightly increased since more weighting was set

Table 3
Results of the power optimization analysis.

Approach	e, deg	AOS, s	FPA, deg	E, W
WLS	n/a	n/a	n/a	n/a
NLWLS (equal)	1.280	1.63	4.592	3.921
NLWLS (power)	1.709	1.75	3.330	3.478
NLWLS (opt)	1.300	1.65	5.047	3.536

on the power consumption, which is mainly affected by the movement of the other actuators, rather than offloading the FPA.

In the proposed scenario, the optimization of secondary objectives in relation to mission needs was successfully demonstrated through the reduction of system level power consumption by 12.1% peak-to-peak and 10.3% on average, while maintaining an acquisition time tolerance of 1.2% and a tracking performance at microradian level.

4. Conclusion

The growing demand for constellations with multiple optical terminals in satellite-based FSOC systems makes advanced control allocation strategies increasingly important. This paper proposes an adapted dynamic control allocation which is tailored to the unique requirements of over-actuated laser communication terminals. This method considers the dynamics and constraints of individual actuators, providing a comprehensive view of the system. It allows for a modular design that incorporates the host satellite platform because the dynamic characteristics of a potential new actuator subsystem can be used to retune the entire system with this model-based approach. The NLWLS was introduced to account for non-linearities resulting from coordinate system transformations, which otherwise leads to significant allocation errors.

Introducing new tailored objectives and cost functions using weighting matrices allows accounting for limited power, performance requirements and increased lifetime of the components. According to the estimated Pareto fronts, future laser communication systems would benefit from higher-bandwidth CPAs and FPAs with higher RBPs while maintaining the size, weight, and power constraints of CubeSat applications.

Specifically, the proposed approach has resulted in maintaining a mean pointing error at 1.280 degrees to 1.300 degrees, representing a minor impact since the tracking error after settling remains at microradian level. The peak-to-peak power consumption has been reduced from 30.5 A to 26.9 A, representing a 12.1% reduction. The mean power consumption has been reduced from 3.9 A to 3.5 A, representing a 10.3% reduction. At the same time, the duration to AOS has been kept almost constant changing from 1.63 s to 1.65 s, representing a 1.2% deviation.

Control allocation can be applied to a wide range of applications, including the demonstrated multi-link. The obtained results will be used to develop dedicated hardware in the OSIRIS framework and to implement it for hardware validation.

CRediT authorship contribution statement

René Rüeddenklau: Writing – review & editing, Writing – original draft, Visualization, Methodology, Formal analysis, Conceptualization. **Georg Schitter:** Writing – review & editing, Supervision.

Declaration of competing interest

The authors declare the following financial interests/personal relationships which may be considered as potential competing interests: René Rüddenklau reports financial support was provided by Bayrische Transformations- und Forschungsstiftung. If there are other authors, they declare that they have no known competing financial interests or personal relationships that could have appeared to influence the work reported in this paper.

Acknowledgments

Funded by the Bavarian Transformation and Research Foundation (Bayrische Transformations- und Forschungsstiftung).

References

[1] T.A. Johansen, T.I. Fossen, Control allocation—A survey, Automatica 49 (5) (2013) 1087–1103.
[2] O. Härkegård, Backstepping and Control Allocation with Applications to Flight Control: Zugl.: Linköping, Univ., Diss., 2003, Linköping Studies in Science and Technology Dissertations, vol. 820, Univ, Linköping, 2003.
[3] O. Härkegård, S.T. Glad, Resolving actuator redundancy—optimal control vs. control allocation, Automatica 41 (1) (2005) 137–144.
[4] A. Dietrich, C. Ott, Hierarchical impedance-based tracking control of kinematically redundant robots, IEEE Trans. Robot. 36 (1) (2020) 204–221.
[5] Y. Zhang, Z. Chen, A closed-loop control allocation method for satellite precision pointing, in: IEEE 10th International Conference on Industrial Informatics, IEEE, 2012, pp. 1108–1112.
[6] Q. Hu, X. Tan, Dynamic near-optimal control allocation for spacecraft attitude control using a hybrid configuration of actuators, IEEE Trans. Aerosp. Electron. Syst. 56 (2) (2020) 1430–1443.
[7] R. Caverly, S. Di Cairano, A. Weiss, Control allocation and quantization of a GEO satellite with 4dof gimbaled thruster booms, in: AIAA Scitech 2020 Forum, American Institute of Aeronautics and Astronautics, Reston, Virginia, 2020.
[8] W.A. Kishore, S. Dasgupta, G. Ray, S. Sen, Control allocation for an over-actuated satellite launch vehicle, Aerosp. Sci. Technol. 28 (1) (2013) 56–71.
[9] J. Jin, B. Park, Y. Park, M.-J. Tahk, Attitude control of a satellite with redundant thrusters, Aerosp. Sci. Technol. 10 (7) (2006) 644–651, [Online]. Available: https://www.sciencedirect.com/science/article/pii/S1270963806000514.
[10] P. Tacx, R. Habraken, G. Witvoet, M. Heertjes, T. Oomen, Identification of an overactuated deformable mirror system with unmeasured outputs, Mechatronics 99 (2024) 103158, [Online]. Available: https://www.sciencedirect.com/science/article/pii/S0957415824000230.
[11] H. Chang, P. Huang, Y. Zhang, Z. Meng, Z. Liu, Distributed control allocation for spacecraft attitude takeover control via cellular space robot, J. Guid. Control Dyn. 41 (11) (2018) 2499–2506.
[12] X. Lang, A. de Ruiter, A control allocation scheme for spacecraft attitude stabilization based on distributed average consensus, Aerosp. Sci. Technol. 106 (2020) 106173.
[13] W. Liu, Y. Geng, B. Wu, J.D. Biggs, Distributed constrained control allocation for cellularized spacecraft attitude control system, J. Guid. Control Dyn. 45 (2) (2022) 385–393.
[14] C. Fuchs, D. Laidlaw, F. Moll, J. Poliak, C. Schmidt, A. Shrestha, Recent results in optical satellite link research at DLR, in: H. Hemmati, B.S. Robinson (Eds.), Free-Space Laser Communications XXXVII, SPIE, 2025, p. 2, [Online]. Available: https://www.spiedigitallibrary.org/conference-proceedings-of-spie/13355/3040371/Recent-results-in-optical-satellite-link-research-at-DLR/10.1117/12.3040371.full.
[15] O. Härkegård, Dynamic control allocation using constrained quadratic programming, J. Guid. Control Dyn. 27 (6) (2004) 1028–1034.
[16] Micro-Epsilon, FSM3000, 2025, [Online]. Available: https://www.micro-epsilon.de/applikationen/branchen/aerospace/spiegel-verkippungssystem-satellitenkommunikation/. (Accessed 25 July 2025).
[17] S.V. Weston, C.D. Burkhard, J.M. Stupl, R.L. Ticknor, B.D. Yost, R.A. Austin, P. Galchenko, L.K. Newman, L. Santos Soto, State-Of-The-Art Small Spacecraft Technology, NASA/TP NASA/TP—20250000142, National Aeronautics and Space Administration, Ames Research Center, Moffett Field, CA 94035-1000, 2025, [Online]. Available: https://www.nasa.gov/smallsat-institute/sst-soa/.
[18] J.C. McDowell, The low earth orbit satellite population and impacts of the SpaceX starlink constellation, Astrophys. J. Lett. 892 (2) (2020) L36.
[19] B. Koosha, P. Madani, M.D. Ardakani, Comprehensive analysis of recent LEO satellite constellations: Capabilities and innovative trends, in: 2025 IEEE Aerospace Conference, IEEE, 2025, pp. 1–12.
[20] R. Rüddenklau, H. Zeihsel, L.R. Rodeck, Trajectory control of a gimbaled prism for hemispherical pointing in CubeSat optical communications, 2025, [Manuscript submitted for publication].
[21] R. Rüddenklau, F. Rein, C. Roubal, B. Rödiger, C. Schmidt, In-orbit demonstration of acquisition and tracking on OSIRIS4CubeSat, Opt. Express 32 (23) (2024) 41188–41200.
[22] S. Dwik, G. Sasikala, S. Natarajan, Advancements and applications of position-sensitive detector (PSD): a review, Optoelectron. Lett. 20 (6) (2024) 330–338.
[23] R. Kingsbury, J. Twichell, S. Palo, Cobalt optical crosslink terminal, in: H. Hemmati, B.S. Robinson (Eds.), Free-Space Laser Communications XXXIV, in: Proceedings of SPIE, SPIE, Bellingham, Washington, USA, 2022, p. 31, [Online]. Available: https://www.spiedigitallibrary.org/conference-proceedings-of-spie/11993/2610501/Cobalt-optical-crosslink-terminal/10.1117/12.2610501.full.

[24] C. Fuchs, C. Schmidt, B. Rödiger, A. Shrestha, M. Brechtelsbauer, J.R. Molina, J. Pacheco, V. Gstaiger, DLR's free space experimental laser terminal for optical aircraft downlinks, in: H. Hemmati, D.M. Boroson (Eds.), Free-Space Laser Communication and Atmospheric Propagation XXIX, Vol. 10096, International Society for Optics and Photonics, 2017, 1009610, http://dx.doi.org/10.1117/12.2254791, SPIE.

[25] E. Csencsics, G. Schitter, Exploring the Pareto fronts of actuation technologies for high performance mechatronic systems, IEEE/ASME Trans. Mechatronics 26 (2) (2021) 1053–1063.

[26] Blue Canyon Technologies, CUBESAT summary, 2025, [Online]. Available: https://www.bluecanyontech.com/wp-content/uploads/3U-1_2025.pdf. (Accessed 22 July 2025).

[27] L. Kramer, J. Peters, R. Voorhoeve, G. Witvoet, S. Kuiper, Novel motorization axis for a coarse pointing assembly in optical communication systems, IFAC Pap. 53 (2) (2020) 8426–8431.

[28] R. Rüddenklau, A. Sinn, G. Schitter, Comparison of high performance hybrid variable reluctance fast steering mirrors, in: 2024 12th International Conference on Control, Mechatronics and Automation, ICCMA, IEEE, 2024, pp. 367–373.

[29] Physik Instrumente (PI) SE & Co KG, S-331 high-dynamics fast steering mirror piezo tip/tilt rapid response, 2025, [Online]. Available: https://www.physikinstrumente.com/en/products/nanopositioning-piezo-flexure-stages/piezo-flexure-tilting-mirrors/s-331-high-speed-tiptilt-platform-300705#specification. (Accessed 22 July 2025).

[30] Optotune, Dual axis fast steering mirror with position feedback - MR-15-30, 2025, [Online]. Available: https://www.optotune.com/mr1530. (Accessed 22 July 2025).

[31] E. Csencsics, G. Schitter, Parametric PID controller tuning for a fast steering mirror, in: 2017 IEEE Conference on Control Technology and Applications, CCTA, 2017, pp. 1673–1678.

[32] G. Wu, S. Zhang, Real-time jerk-minimization trajectory planning of robotic arm based on polynomial curve optimization, Proc. Inst. Mech. Eng. Part C: J. Mech. Eng. Sci. 236 (21) (2022) 10852–10864.

[33] R. Rüddenklau, B. Rödiger, C. Roubal, C. Schmidt, F. Moll, Vibration load compliance of a miniaturized CubeSat quantum communication terminal, J. Vib. Control 10775463251366143, http://dx.doi.org/10.1177/10775463251366143.

[34] K. Levenberg, A method for the solution of certain non-linear problems in least squares, Quart. Appl. Math. 2 (2) (1944) 164–168.

[35] D.W. Marquardt, An algorithm for least-squares estimation of nonlinear parameters, J. Soc. Ind. Appl. Math. 11 (2) (1963) 431–441.